Available online at www.sciencedirect.com

SciVerse ScienceDirect

Ceramics International 39 (2013) 2283–2292

CERAMICS INTERNATIONAL

www.elsevier.com/locate/ceramint

XPS and optical studies of different morphologies of ZnO nanostructures prepared by microwave methods

R. Al-Gaashani[a,b,*], S. Radiman[a], A.R. Daud[a], N. Tabet[c], Y. Al-Douri[d]

[a]School of Applied Physics, Faculty Science and Technology, Universiti Kebangsaan Malaysia, 43600 Bangi, Selangor, Malaysia
[b]Department of Physics, Thamar University, Dhamar, Republic of Yemen
[c]Department of Physics, Center of Research Excellence in Renewable Energy, King Fahd University of Petroleum and Minerals, Dhahran, Saudi Arabia
[d]Institute of Nano Electronic Engineering, University Malaysia Perlis, 01000 Kangar, Perlis, Malaysia

Received 26 July 2012; received in revised form 25 August 2012; accepted 26 August 2012
Available online 8 September 2012

Abstract

Zinc oxide (ZnO) nanostructures of various morphologies were prepared using a microwave-assisted aqueous solution method. Herein, a comparative study between three different morphologies of ZnO nanostructures, namely nanoparticles (NPs), nanoflowers (NFs) and nanorods (NRs) has been reviewed and presented. The morphologies of the prepared powders have been studied using field effect scanning electron microscopy (FESEM). X-ray diffraction (XRD) results prove that ZnO nanorods have biggest crystallite size compared with nanoflowers and nanoparticles. The texture coefficient (T_c) of three morphologies has been calculated. The T_c changed with varying morphology. A comparative study of surfaces of NPs, NFs and NRs were investigated using X-ray photoelectron spectroscopy (XPS). The possible growth mechanisms of ZnO NPs, NFs and NRs have been described. The optical properties of the ZnO nanostructures of various morphologies have been investigated and showed that the biggest crystallite size of ZnO nanostructures has lowest band gap energy. The obtained results are in agreement with experimental and theoretical data of other researchers.

Keywords: A. Microwave processing; B. Grain size; C. Optical properties; D. ZnO

1. Introduction

Zinc oxide (ZnO) has attracted a great deal of interest due to its electronic properties. It is a semiconductor with a wide band gap (3.4 eV) that is used as a substrate for the growth of other semiconductors such as GaN and SiC [1] applicable for optoelectronics [2–4]. ZnO nanostructures have been used for fabrication of a wide variety of devices [5,6] including light emitting diodes, laser diodes and field emission devices [7,8], piezoelectric devices [9], photovoltaic devices [10], catalysis [11], hybrid solar cells [12,13] and gas sensors [14,15].

Different techniques have been used by many authors to synthesize various ZnO nanostructures. Recently, Rezapour and Talebian [16] have synthesized crystalline ZnO with different morphologies by solvothermal and sol–gel synthesis methods in various solvents as the reaction medium and studied the photocatalytic activity of the prepared nanostructures. Lu et al. [17] have shown that the optical transmittance of Al-doped ZnO films can be improved using ZnO nanorods synthesized by aqueous chemical growth technique, where the length and diameter of the rods were controlled by the OH^- concentration of hexamethenamine in the solution. Lastly, Tsai et al. [18] have studied the effect of ultraviolet treatment on the structural and optical properties of ZnO nanoparticles and showed that ultraviolet treatment may induce the formation of surface oxygen vacancies leading to hydroxyl adsorption.

In this work, we report on green methods that allow the synthesis of ZnO nanostructures with different morphologies, namely nanoparticles (NPs), nanoflowers (NFs) and nanorods (NRs) using aqueous solution exposed to microwave radiation. Possible growth mechanisms of three morphologies

*Corresponding author at: Universiti Kebangsaan Malaysia, School of Applied Physics, Faculty Science and Technology, 43600 Bangi, Selangor, Malaysia. Tel.: +60 173981135; fax: +60 3 89269470.
E-mail address: Rashad_jashani@yahoo.com (R. Al-Gaashani).

0272-8842/$ - see front matter
http://dx.doi.org/10.1016/j.ceramint.2012.08.075

of the ZnO nanostructures have been suggested based on the interaction of microwaves with materials. The structural and optical properties of the prepared nanostructures have been investigated using X-ray diffraction, XPS, FESEM and UV–vis absorption spectroscopy. In addition, we present a detailed comparative study of XPS results and optical properties of three morphologies (NPs, NFs and NRs) of ZnO nanostructures. To the best of our knowledge, such correlation has not been reported in the literature.

2. Experimental

2.1. Materials

The zinc cation precursor chemical materials used for the synthesis of ZnO samples were zinc chloride ($ZnCl_2$), zinc acetate dehydrate ($ZnC_4H_6O_4 \cdot 2H_2O$) and zinc nitrate tetrahydrate ($ZnN_2O_6 \cdot 4H_2O$). Sodium hydroxide (NaOH) was used as the hydroxide anion precursor. All raw chemicals were from Aldrich Fluka (Aldrich Chemical Co) with purity better than 99%. Deionized water (DIW) (resistivity 18.2 MΩ cm) was used as a solvent. Microwave processing was done using a conventional microwave oven (Model No. EM-G430, 2.45 GHz, maximum output power 1000 W, SANYO Electric, UK) equipped with six power levels.

2.2. Preparation of ZnO nanoparticles

ZnO nanoparticles were synthesized via a microwave-assisted aqueous solution method (MWASM). In a typical experiment, 0.9 g of $ZnCl_2$ was dissolved in 100 ml deionized water under magnetic stirring at room temperature for 5 min to form the aqueous solution of $ZnCl_2$, named as aqueous solution-A. Similarly, 1.4 g of NaOH was dissolved in 20 ml deionized water under magnetic stirring at room temperature for 5 min to form the aqueous solution of NaOH, named as aqueous solution-B. Then, the aqueous solution-B was added dropwise to the aqueous solution-A under magnetic stirring until a milky solution of $pH_f = 13.75$ at 24.9 °C resulted. After 1 h stirring, the final mixture solution was transferred into a flat-bottom flask (500 ml). Then, the flask was put into the microwave oven to irradiate the mixture solution for 2 min with the microwave power set at 1000 W. The hot solution with a white precipitate was left to cool down naturally to room temperature (RT). Subsequently, the solution was filtered and separated by centrifugation at 4000 rpm for 10 min, washed with DIW and absolute ethyl alcohol several times to remove the impurities, and finally dried in air at 60 °C for 24 h. The obtained powder was heated at 300 °C for 2 h in a conventional oven.

2.3. Preparation of ZnO nanoflowers

Flower shaped ZnO nanostructures were synthesized by MWASM. Some authors obtained ZnO flowers-like similar to our product using different methods and conditions [19–22]. A similar morphology was obtained in aqueous solution assisted by sonication assisted with stirring for 4 h at 80 °C [19]. In our typical experiment, 0.9 g of $Zn(NO_3)_2 \cdot 6H_2O$ was dissolved in 100 ml deionized water under magnetic stirring at room temperature for 5 min to form the aqueous solution of $Zn(NO_3)_2 \cdot 6H_2O$, named as aqueous solution-A. Similarly, 0.27 g of NaOH was dissolved in 20 ml deionized water under magnetic stirring at room temperature for 5 min to form the aqueous solution of NaOH, named as aqueous solution-B. Then, the aqueous solution-B was added dropwise with 2 ml pyridine (C_5H_5N), as a basic additive which plays an important role of controlling of the ZnO morphology, to the aqueous solution-A under magnetic stirring until a milky solution of $pH_f = 13.5$ at 28.5 °C resulted. After 2 h stirring, the final mixture solution was transferred into a flat-bottom flask (500 ml). Then, the flask was put inside the microwave oven to irradiate the mixture solution under air for 2 min duration with the microwave power set at 1000 W. The hot solution with a white precipitate was left to cool down to RT. After that the cooled solution was separated by centrifugation at 4000 rpm for 10 min, washed with DIW and absolute ethyl alcohol several times to remove the impurities, and finally dried in air at 60 °C for 24 h.

2.4. Preparation of ZnO nanorods

In a typical experiment, 0.149 M (100 ml) of zinc acetate dehydrate ($ZnC_4H_6O_4 \cdot 2H_2O$) and 3.33 M (30 ml) of NaOH aqueous solutions were prepared in deionized water (DIW, resistivity 18.2 MΩ cm) under magnetic stirring at 30 °C. After stirring for 5 min of the zinc acetate aqueous solution, the NaOH aqueous solution was gradually added dropwise under constant magnetic stirring until a milky solution was resulted. After 60 min stirring, the final mixture solution was transferred into a flat-bottom flask 500 ml. Then, the flask was put inside the microwave oven to irradiate the mixture solution under air for 5 min duration (on/off) with the power set at 1000 W. The resulting hot solution with a white precipitate was left to cool down to RT naturally. Then the white precipitate was separated by centrifugation at 4000 rpm for 5 min, washed with DIW and ethyl alcohol several times, and finally dried in air at 60 °C for 24 h. The obtained powder was heated at 500 °C for 2 h in a conventional oven.

2.5. Methods

The structural characterization of all samples was carried out by X-ray powder diffraction (XRD), using a Bruker-AXSD8 advance X-ray diffractometer with Cu-K_α radiation source ($\lambda = 1.5418$ Å). The morphology of the samples at the nanoscale was observed using a SUPRA 55VP field emission scanning electron microscope (FESEM).

All samples were analyzed by X-ray photoelectron spectroscopy (XPS) using XSAM-HS KRATOS electron spectrometer. The binding energies were corrected for the

charge shift using the C 1s peak of graphitic carbon (BE = 284.6 eV) as a reference. The atomic concentrations of all the elements (O and Zn) were determined using a dedicated software (Kratos Vision software, AXIS Ultra 'DLD').

The optical properties were investigated by recording the (UV–vis) absorption spectra at room temperature using a Perkin-Elmer Lambda 35 spectrophotometer in the 250–1100 nm wavelength range and a 10 mm quartz cuvette.

3. Results and discussion

3.1. Structural and morphology of ZnO nanostructures

Fig. 1 shows the XRD patterns of ZnO nanoparticles, nanoflowers and nanorods. The XRD analysis results confirmed that all prepared powders with their various morphologies correspond to a pure phase of ZnO wurtzite structure, with a hexagonal crystal system (space group $P63mc$, $a=b=3.25010$ Å, $c=5.20710$ Å, $\alpha=\beta=90^\circ$ and $\gamma=120^\circ$; JCPDS card no. 01-079-2205). It is clear that the XRD pattern of ZnO nanorods has the highest intensity (the amount of crystalline phase) resulting from a high crystallinity of ZnO nanorods compared with other morphologies because it was treated at 500 °C for 2 h in a conventional furnace.

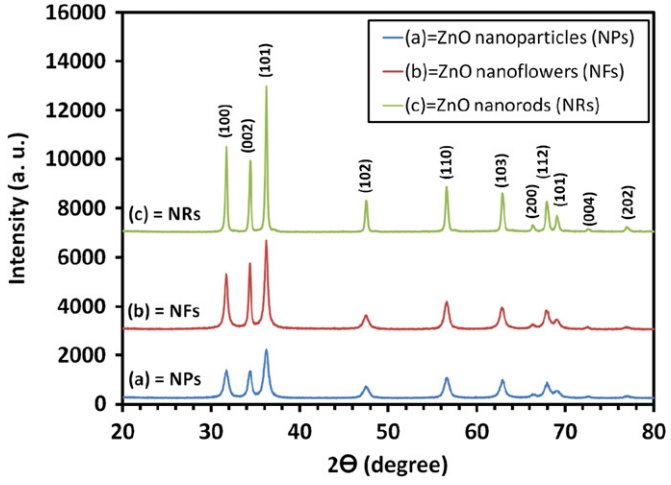

Fig. 1. XRD patterns of ZnO (a) nanoparticles; (b) nanoflowers and (c) nanorods synthesized via microwave-assisted aqueous solution methods.

The full-width at half-maximum β (in radian) of the main diffraction peak (1 0 1) was used to calculate the crystallite size of the samples using Scherrer's equation:

$$t = \frac{0.9\,\lambda}{\beta \cos\theta} \tag{1}$$

where θ is the diffraction angle, and λ is 1.54 Å of the Cu K_α line. The calculated crystallite sizes of ZnO nanoparticles, nanoflowers and nanorods are 18.6, 23.9 and 46.2 nm, respectively, as given in Table 1.

The preferred crystallite orientation and growth of the ($h\,k\,l$) planes has been studied in terms of the texture coefficient $T_{c(h\,k\,l)}$ defined by Barret and Massalski [25] as:

$$T_{c(h\,k\,l)} = \left(\frac{I_{(h\,k\,l)}}{I_{o(h\,k\,l)}}\right) \Big/ \left[1/n \sum \left(\frac{I_{(h\,k\,l)}}{I_{o(h\,k\,l)}}\right)\right] \tag{2}$$

in which $I_{(h\,k\,l)}$ is the measured XRD intensities of corresponding planes ($h\,k\,l$) obtained from the samples, $I_{o(h\,k\,l)}$ is the standard intensities of the XRD pattern references of the corresponding powders given in (JCPDS card no. 079-2205) and n is the number of diffraction planes (peaks). It is worth mentioning that Eq. (2) provides useful information only if the number of peaks is considered.

The texture coefficient (T_c) of the main nine ($h\,k\,l$) planes of ZnO NPs, NFs and NRs is listed in Table 2. One can notice that a value of $T_{c(h\,k\,l)}$ greater than unity indicates the abundance of grains in that [$h\,k\,l$] direction whereas a value of $T_{c(h\,k\,l)}$ equals to unity for all measured ($h\,k\,l$) planes means a randomly oriented crystallite like in the JCPDS reference [26]. From Table 2, we can conclude that the highest values of $T_{c(h\,k\,l)}$ are $T_{c(0\,0\,2)}$ for the three morphologies. These values are 1.13, 1.76 and 1.17 for ZnO NPs, NFs and NRs, respectively. Thus, the preferred crystallite orientation in three morphologies is [0 0 2] direction which is the highest in case ZnO NFs. On the other hand, the ratio [0 0 2]/[1 0 1] of the three morphologies was calculated from relative intensities of XRD patterns obtained of ZnO NPs, NFs and NRs. These ratios are 0.555, 0.739 and 0.484 for ZnO NPs, NFs and NRs, respectively. These values are higher than the theoretical ratio of [0 0 2]/[1 0 1] = 0.415 as given in JCPDS card no. 079-2205 for a random orientation of the crystallites.

Fig. 2 shows FESEM images of ZnO nanoparticles prepared by microwave-assisted aqueous solution method

Table 1
The crystallite size; the band gap of various morphologies of ZnO nanostructures synthesized via microwave-assisted aqueous solution methods under different conditions.

ZnO sample	Morphology nano-	Microwave duration at 1000 W (min)/conventional heating (°C) for (2 h)	Crystallite size (Scherrer); D_{101} (nm)	Band gap E_g (eV)
ZnO	Particles	2/300	18.6	3.40; 3.44[a]; 1.57[b]
ZnO	Flowers	2/No	23.9	3.25
ZnO	Rods	5/500	46.2	3.12

[a] Ref. [23] Exp.
[b] Ref. [24] Theor.

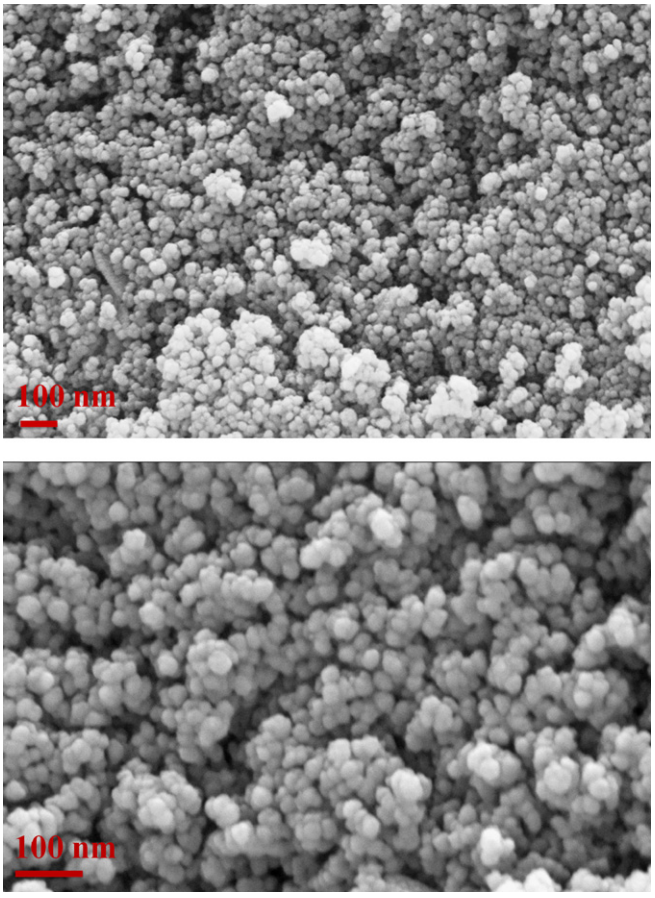

Fig. 2. FESEM images of ZnO nanoparticles synthesized via microwave-assisted aqueous solution methods within 2 min at 1000 W.

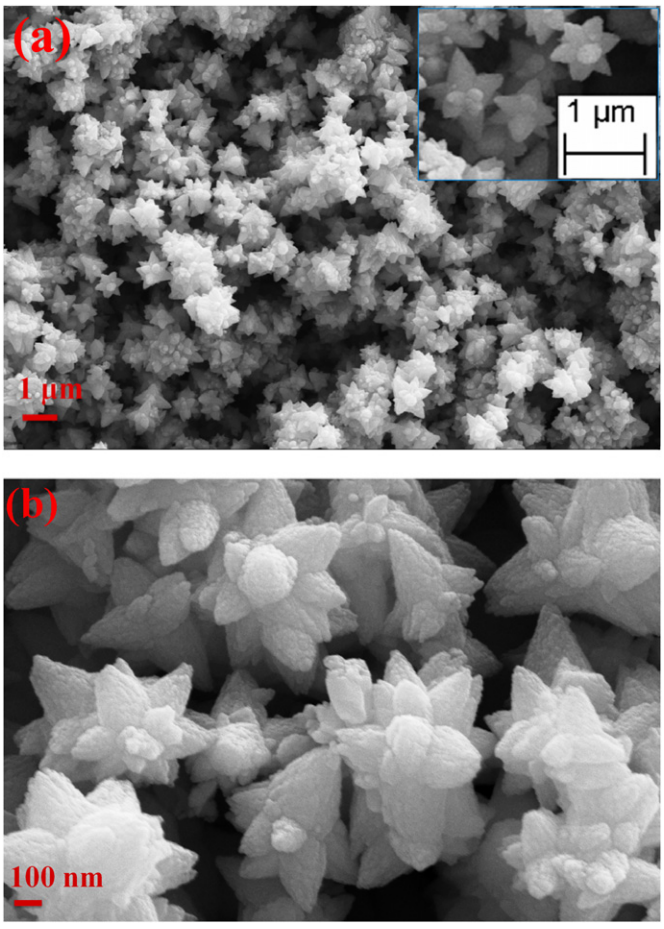

Fig. 3. FESEM images of ZnO nanoflowers synthesized via microwave-assisted aqueous solution methods within 2 min at 1000 W.

using $ZnCl_2$ and NaOH within 2 min at 1000 W. It is cleared that the nanoparticles are approximately spherical and irregular in shape and size. This result may be due to the product was filtered and post-annealed at 300 °C for 2 h by a conventional furnace [27]. It is noted that the surfaces of ZnO nanoparticles are very smooth due probably to the post-annealing treatment [28].

The possible chemical reactions leading to the formation of the ZnO nanoparticles have been described in details elsewhere [29]. The possible growth mechanism of ZnO nanoparticles prepared by microwave-assisted aqueous solution methods under microwave radiation could be as follows: Firstly, the initial ZnO crystal nuclei act as dipoles in the mixture solution under the effect of the electric field of microwave radiation. Then, under exposure to microwave power (1000 W) for 2 min, the obtained ZnO nuclei polarize and aggregate to form ZnO nanoparticles. ZnO nanoparticles with spherical shapes and smooth surfaces were obtained, possibly due to the post-annealing treatment at 300 °C for 2 h in the furnace [28].

Fig. 3 shows FESEM images of flowers shaped ZnO nanostructures synthesized via the microwave-assisted aqueous solution method using $Zn(NO_3)_2 \cdot 6H_2O$, NaOH and pyridine as a modifying agent within 2 min at 1000 W. The inserted image in Fig. 3 (a) indicates that each unit of flower-shaped ZnO nanostructures has a receptacle, six petals grown in the medial part of the receptacle and a stigma. The lengths of flower-shaped ZnO nanostructures are in the range of 0.8–2 μm. The width of each petal varies from the tip to the basis. The widths of the tip and basis are in the range of 100–200 and 250–400 nm, respectively. Each part of flower-shaped ZnO nanostructure consists of very small nanoparticles as shown in Fig. 3(b).

The possible growth mechanism of flower-shaped ZnO nanostructure is shown in Fig. 4 which shows the initial ZnO crystal nucleus structure with its different planes. During the stirring, there is a possibility for the following reversible reaction to occur [29]:

$$Zn(OH)_2 + 2OH^- \overset{\text{stirring at } 25\ ^\circ C}{\leftrightarrow} Zn(OH)_4^{2-} \quad (3)$$

The negative growth units ($Zn(OH)_4^{2-}$) can easily form in the strong basic medium as in our case, $pH_f = 13.5$. According to this reaction and the availability of rich Zn^{2+} ions in the medium, the negative ($Zn(OH)_4^{2-}$) ions are easily attracted by the positive polar planes (0 0 0 1) made of Zn^{2+} [19]. Some growth units ($Zn(OH)_4^{2-}$) can react with OH^- groups on the initial ZnO crystal nuclei surfaces to allow more nucleation and growth in the *c*-axis

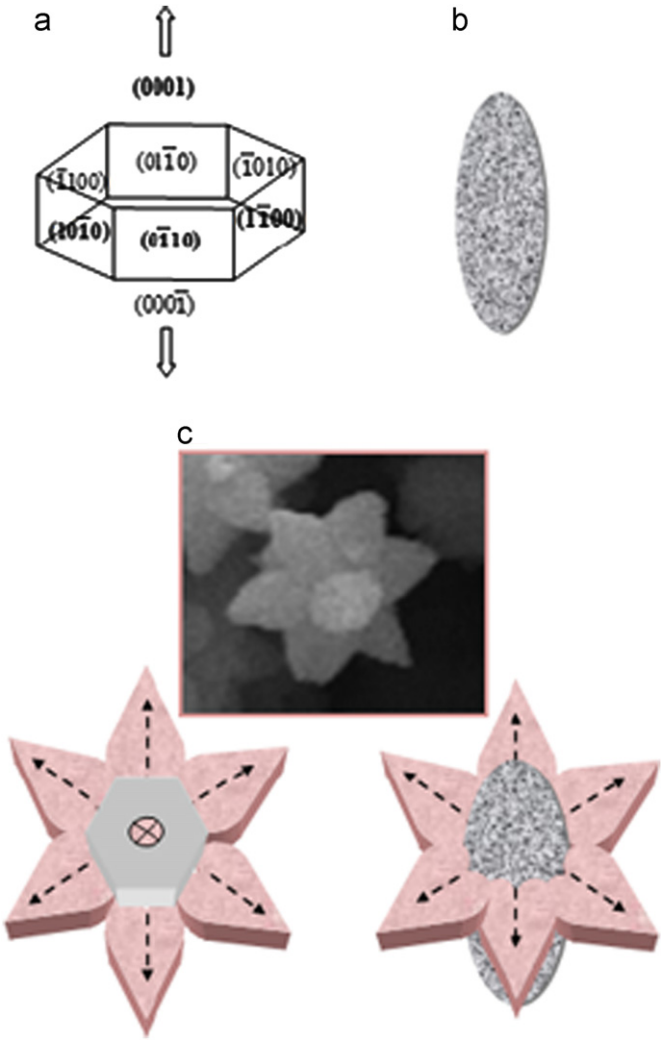

Fig. 4. Growth schematic diagrams of the possible growth mechanism of flower-shaped ZnO nanostructures.

direction. In this case, ZnO rod-like with hexagonal shape will grow in the *c*-axis direction. However, the growth of ZnO rod-like along the positive planes may be limited because pyridine (py) molecules (C_5H_5N) which can react with Zn^{2+} ions on the positive polar surfaces to form pyridine complexes of zinc (py–Zn^{2+} complexes). So, the pyridine molecules act as a capping agent layer on the positive polar surfaces of ZnO structure. When the adsorbed molecules of pyridine on the positive plane (0 0 0 1) of ZnO increase, the surface energy of (0 0 0 1) plane will be reduced. Thus, the growth rate along the [0 0 0 1] direction will decrease and the thickness of the rod-like ZnO will increase with steadily decreasing the top part of the rod to form rugby-like ZnO nanostructures with sharp ends due to the diffusion-limited growth under the capping agent [19,30] as shown in Fig. 4(b). Subsequently the growth process proceeds in the middle of the rugby-like ZnO structure from the six facets of hexagonal wurtzite crystal to form six petals of the flower-shaped ZnO nanostructures. Each petal is half rugby-like and grows in the [0 0 0 1] direction of the *c*-axis as shown in Fig. 4(c). The basic additives such as pyridine, triethanolamine and aniline were previously used to control the morphology of ZnO nanostructures because of these additives have various reactions and different adsorption ability on various surfaces of ZnO crystal, leading to a significant change in the growth rates of different crystal facets and directions [19,31].

The growth mechanism of the ZnO nanorods can be described as follows: the initial ZnO crystal nucleus structure with its different planes is shown in Fig. 3(a). As discussed previously, the negative growth units, $(Zn(OH)_4^{2-})$ can easily form in the strong basic medium as in our case, $pH_f = 12.2$. According to Eq. (1) and the availability of rich Zn^{2+} ions in the medium, the $(Zn(OH)_4^{2-})$ ions are attracted by the positive polar planes (0 0 0 1) of Zn^{2+}. Some growth units $(Zn(OH)_4^{2-})$ can react with OH^- groups on the initial ZnO crystal nuclei surfaces to allow more nucleation and growth in the *c*-axis direction.

Fig. 5 displays FESEM images of ZnO nanorods (NRs) synthesized via microwave-assisted aqueous solution method using Zinc acetate dihydrat ($ZnC_4H_6O_4 \cdot 2H_2O$) and NaOH within 5 min at 1000 W. The hexagonal nanorods (pencils-like) have average diameters of about 45–96 nm and lengths around 0.5–1 μm (Fig. 5(b)). Each nanorod has almost the same diameter throughout its length and exhibited smooth surfaces. The inserted image in Fig. 5(b) shows the tip of nanorods at high magnification.

3.2. XPS analysis of different morphologies of ZnO nanostructures

The ZnO nanostructures were analyzed by X-ray photoelectron spectroscopy (XPS). Fig. 6 shows the typical XPS wide survey spectra of various morphologies of ZnO (a) nanoparticles, (b) nanoflowers and (c) nanorods. Zn, O and C peaks were detected as shown in the three wide survey spectra in Fig. 6. The detected carbon is related to the carbon adsorbed on the surface during the exposure of the sample to the ambient atmosphere. All binding energies were corrected for the charge shift using the C 1s peak of graphitic carbon (BE = 284.6 eV) as a reference [32].

Fig. 7 demonstrates the comparison of raw data of high resolution XPS spectra of the Zn 2p region (I) and O 1s core-level (II) of various morphologies of ZnO (a) nanoparticles, (b) nanoflowers and (c) nanorods. From Fig. 7(I), it can be observed that the binding energies of the Zn 2p components are slightly different. This is probably due to various surface morphologies of ZnO nanostructures [33]. The binding energies of the Zn 2p components of ZnO nanorods are significantly higher than the binding energies of the Zn 2p components of ZnO nanoparticles and nanoflowers. The binding energies difference could be attributed to two main possible reasons: (1) the chemical environment interaction with the surface atoms (composition of the 5 nm top thickness of the surface) and (2) the variation of the texture coefficients with morphology as shown in Table 2. Gladys et al. [34]

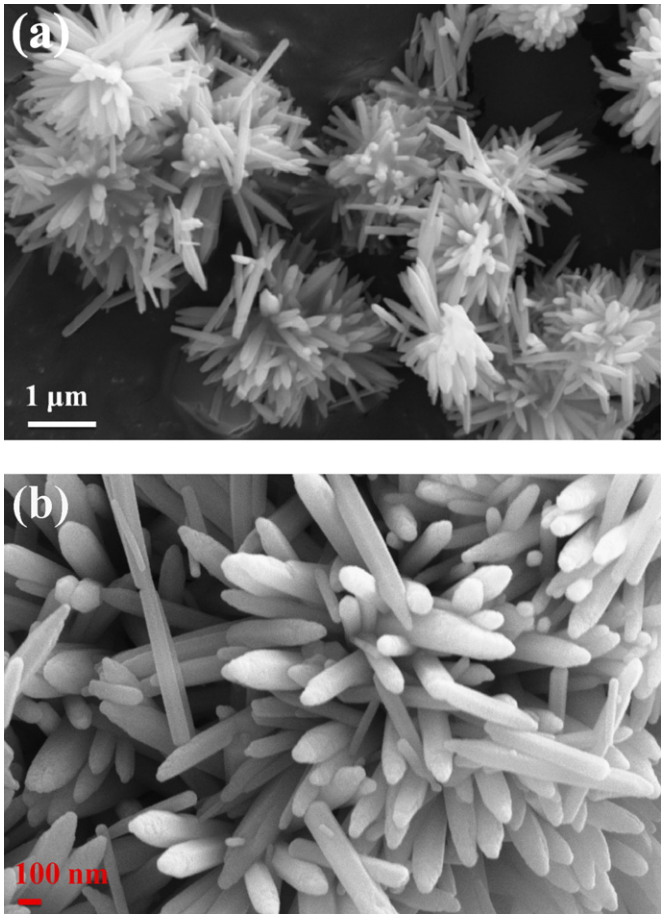

Fig. 5. FESEM images of ZnO nanorods synthesized via microwave-assisted aqueous solution methods within 5 min at 1000 W.

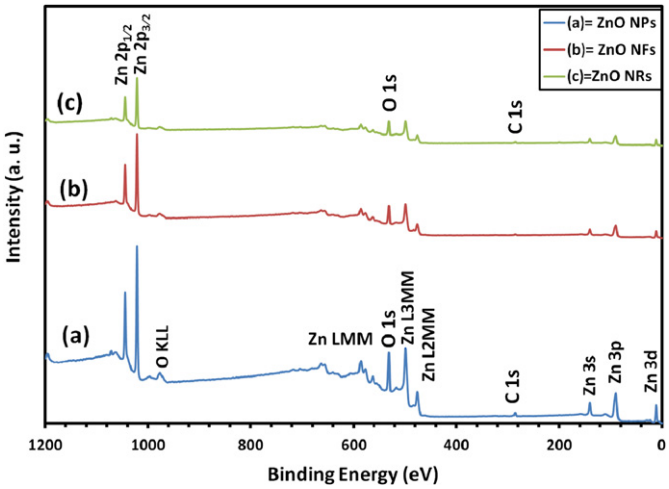

Fig. 6. XPS wide survey spectra of various morphologies of ZnO (a) nanoparticles; (b) nanoflowers and (c) nanorods synthesized via microwave-assisted aqueous solution methods.

have reported that the smaller binding energy shifts of surface core-level in clean and oxygen-covered $I_r(2\,1\,0)$ surfaces are associated with different atomic packing density for {1 1 0} and {3 1 1} facets compared to the atomically rough (2 1 0) surface.

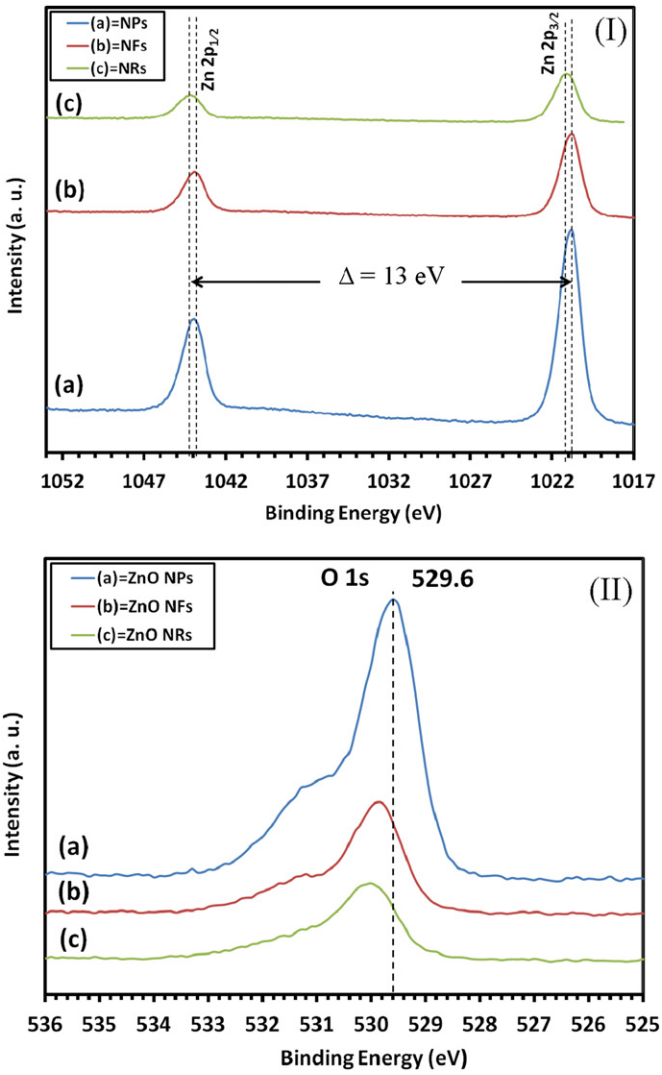

Fig. 7. XPS spectra of raw data of Zn 2p (I) and O 1s (II) of various morphologies of ZnO (a) nanoparticles; (b) nanoflowers and (c) nanorods synthesized via microwave-assisted aqueous solution methods.

From Fig. 7(I) and Table 3, the Zn 2p core-level of ZnO NPs has two fitting peaks located at about 1043.7 and 1020.7 eV attributed to Zn $2p_{1/2}$ and Zn $2p_{3/2}$, respectively. Similarly, those two fitting peaks located at 1043.8 and 1020.8 eV are attributed to Zn $2p_{1/2}$ and Zn $2p_{3/2}$ of ZnO NFs, respectively. However, the Zn 2p core-level of ZnO NRs has two fitting peaks shifted towards the higher binding energy. Those two fitting peaks located at 1044.2 and 1021.2 eV are ascribed to Zn $2p_{1/2}$ and Zn $2p_{3/2}$, respectively [35–37]. These results indicate that the chemical valence of Zn at the surface of three morphologies of ZnO is (+2 oxidation state). Zn $2p_{3/2}$ peak was fitted to only one Gaussian in all samples analyzed. The binding energy difference between the Zn $2p_{1/2}$ and Zn $2p_{3/2}$ is 23 eV for three morphologies of ZnO.

Fig. 8 displays XPS spectra of O 1s region of various morphologies of ZnO (a) nanoparticles, (b) nanoflowers and (c) nanorods. It is demonstrated at Fig. 8(a) that the O 1s core-level spectrum of ZnO nano-particles which shows two

Table 2
The variation of the texture coefficient with morphology.

Morphology of ZnO	Texture coefficient (T_c) of ($h\,k\,l$) planes								
	$T_{c(1\,0\,0)}$	$T_{c(0\,0\,2)}$	$T_{c(1\,0\,1)}$	$T_{c(1\,0\,2)}$	$T_{c(1\,1\,0)}$	$T_{c(1\,0\,3)}$	$T_{c(2\,0\,0)}$	$T_{c(1\,1\,2)}$	$T_{c(2\,0\,1)}$
NPs	0.94	1.13	0.85	0.96	1.01	1.02	0.98	1.03	1.067
NFs	1.06	1.76	0.99	0.68	0.97	0.82	0.89	0.88	0.93
NRs	1.03	1.17	1	0.99	0.99	0.95	0.97	0.92	0.97

Table 3
XPS analysis of various morphologies of ZnO nanoparticles (NPs); nanoflowers (NFs) and nanorods (NRs) synthesized via microwave-assisted aqueous solution methods.

Peak	Position *BE* (eV) $\pm$0.10 eV	FWHM (eV) $\pm$0.20 eV	Raw area (cps eV)	Atomic Conc. (%)
ZnO NPs				
Zn $2p_{1/2}$	1043.7	1.7	189,227.1	16.7
Zn $2p_{3/2}$	1020.7	1.6	370,022.6	33.2
O 1s (1)	529.6	1.1	44,995.1	33.3
O 1s (2)	531.1	1.7	22,658.8	16.8
ZnO NFs				
Zn $2p_{1/2}$	1043.8	1.6	78,933.9	17.1
Zn $2p_{3/2}$	1020.8	1.6	154,856.4	33.9
O 1s (1)	529.7	1.1	18,858.2	34.1
O 1s (2)	531.2	1.6	8,268	14.9
ZnO NRs				
Zn $2p_{1/2}$	1044.2	1.6	48,415.0	15.9
Zn $2p_{3/2}$	1021.2	1.6	92,237.7	30.7
O 1s (1)	530.2	1.1	10,836.2	29.8
O 1s (2)	531.1	1.2	5,531.1	15.2
O 1s (3)	532.3	1.5	3,038.0	8.4

different forms of oxygen. Two fitting Gaussians peaks marked as (1) and (2) were used to fit the experimental data. Peak (1), positioned at the lower binding energy of 529.6 eV, and is assigned to O^{2-} ions in the Zn–O bonding of the wurtzite structure of ZnO [37]. The other peak (2) located at 531.1 eV is related to OH group absorbed onto the surface of the ZnO nanoparticles [33]. Similarly, two fitting Gaussians peaks marked as (1) and (2) were used to fit the raw data of O 1s region of ZnO nanoflowers as shown in Fig. 8(b). The peaks located at 529.7 and 531.2 eV can be ascribed to O^{2-} ions in the Zn–O bonding of the wurtzite structure of ZnO nanoflowers and to the Zn–OH bonding, respectively. This result is in agreement with the previous report of ZnO nanoflowers [35]. However, The O 1s region of ZnO nanorods can be fitted into three Gaussian peaks marked as (1), (2) and (3) as shown in Fig. 8(c). The peak located at 530.2 eV belongs to the Zn–O bonding in ZnO. Peaks located at 531.1 and 532.3 eV can be ascribed to the Zn–OH bonding and to the presence of C=O bonding originated from the surface adsorbed histidine molecules. These values are good in agreement with the previous work of ZnO nanorods [38].

The summary of XPS analysis of ZnO NPs, NFs and NRs is shown in Table 3. Binding energy (BE) in eV for the core levels Zn 2p and O 1s and their corresponding full-width at half maximum (FWHM) along with the respective atomic concentrations are listed in Table 3. The results show that the ratio O/Zn is slightly lower than unity confirming that the synthesized powders are pure ZnO as conformed by XRD results.

3.3. Optical properties of different morphologies of ZnO nanostructures

The optical properties of the different morphologies of ZnO nanostructures were studied by ultraviolet–visible (UV–vis) absorption spectroscopy technique. The optical band gap energy (E_g) of the prepared samples was estimated using Eq. (4) [39,40] and Tauc plot method [41,42]:

$$(\alpha h\nu)^n = B(h\nu - E_g) \tag{4}$$

where α is the absorption coefficient, $h\nu$ is the photo energy, n equals either 1/2 for an indirect transition (indirect band gap semiconductors) or 2 for a direct transition (direct band gap semiconductors) and B is a material-dependent constant. The value of the absorption coefficient can be determined by the following equation [43]:

$$\alpha = \frac{-1}{d}\ln\frac{I_t}{I_o} = \frac{A}{d\log e} \approx 2.303\frac{A}{d} \tag{5}$$

where d is the thickness of the used cuvette (the sample thickness), I_o and I_t are the intensities of incident and

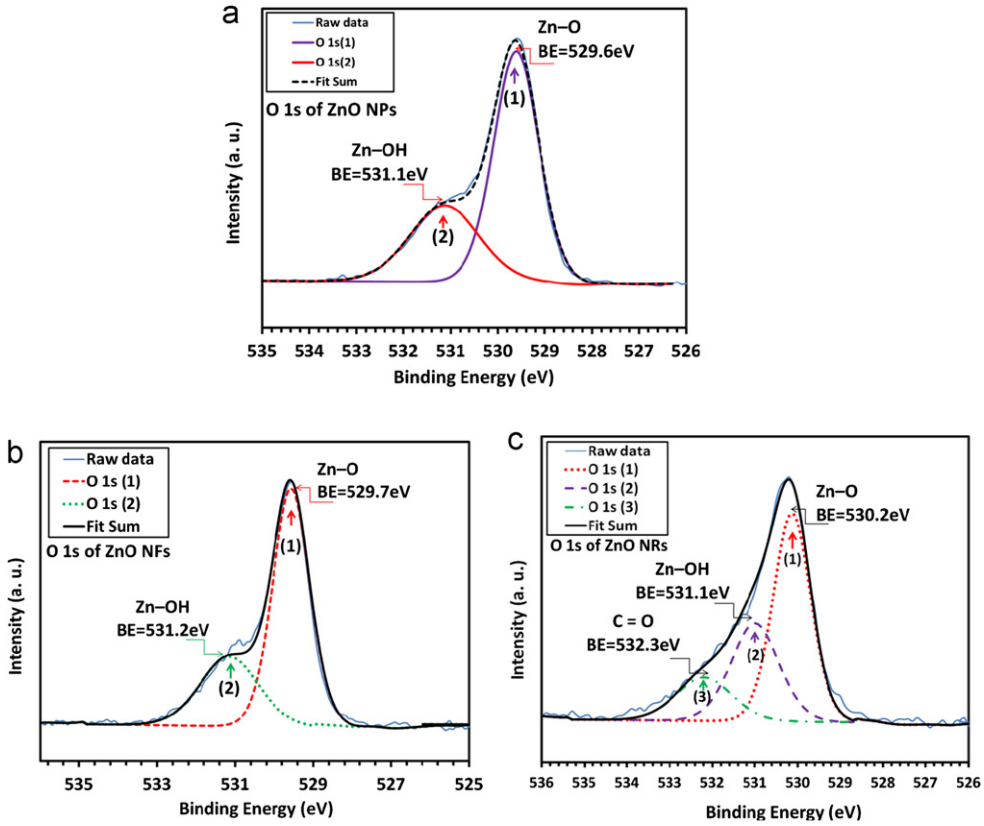

Fig. 8. XPS spectra of O 1s of various morphologies of ZnO (a) nanoparticles; (b) nanoflowers and (c) nanorods.

transmitted light, respectively, $A = \log(I_o/I_t)$ is the absorbance, obtained from the UV–vis absorption spectra.

Fig. 9 shows the UV–vis absorption spectra of various morphologies of ZnO (a) nanoparticles, (b) nanoflowers and (c) nanorods synthesized via microwave-assisted aqueous solution methods. In the UV region, the main absorption peaks of the ZnO samples (a) nanoparticles, (b) nanoflowers and (c) nanorods are about 368 nm (3.37 eV), 370 nm (3.35 eV) and 378 nm (3.28 eV), respectively. It is clearly observed that the absorption peaks showed a blue shift as the crystallite size of the samples decreases. This result is in good agreement with the previous literatures in many semiconductor nanostructures [44,45]. It is worth noting that the absorption curve of ZnO NRs is very different compared to the others. It has high absorption at long wavelength and very slow decrease of the absorption curve at short wavelengths. This could be related to the presence of carbon compounds (C = O) as shown in XPS analysis.

The Plots of $(\alpha h\nu)^2$ against photon energy ($h\nu$) will have a linear region and extrapolation of the straight line to zero absorption gives the energy gap for various morphologies of ZnO nanostructures as shown in Fig. 10(I). The obtained energy gap values are in good agreement with ZnO nanoparticles [46], nanoflowers [47] and nanorods [48]. The increasing of optical band gap values with the decreasing of the grain size as illustrated in Fig. 10(II) could be associated to the electron confinement as observed in

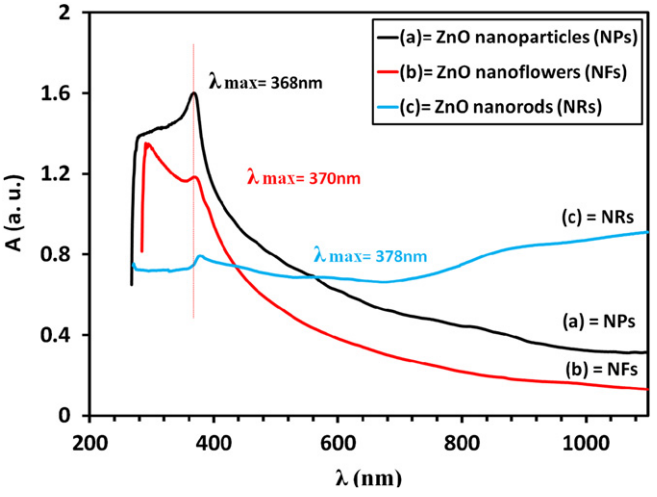

Fig. 9. UV–vis absorption spectra of various morphologies of ZnO (a) nanoparticles; (b) nanoflowers and (c) nanorods synthesized via microwave-assisted aqueous solution methods.

various materials [49]. On the other hand, the energy gap can be expressed as a function of the radius of nanoparticles as follows [50]:

$$E_g^{\text{eff}} = E_g^{\text{bulk}} + \frac{\hbar^2\pi^2}{2\mu R^2} \tag{6}$$

where R is the radius of the particles and μ is the effective reduced mass. The value μ equals 0.275 m_e and m_e is the

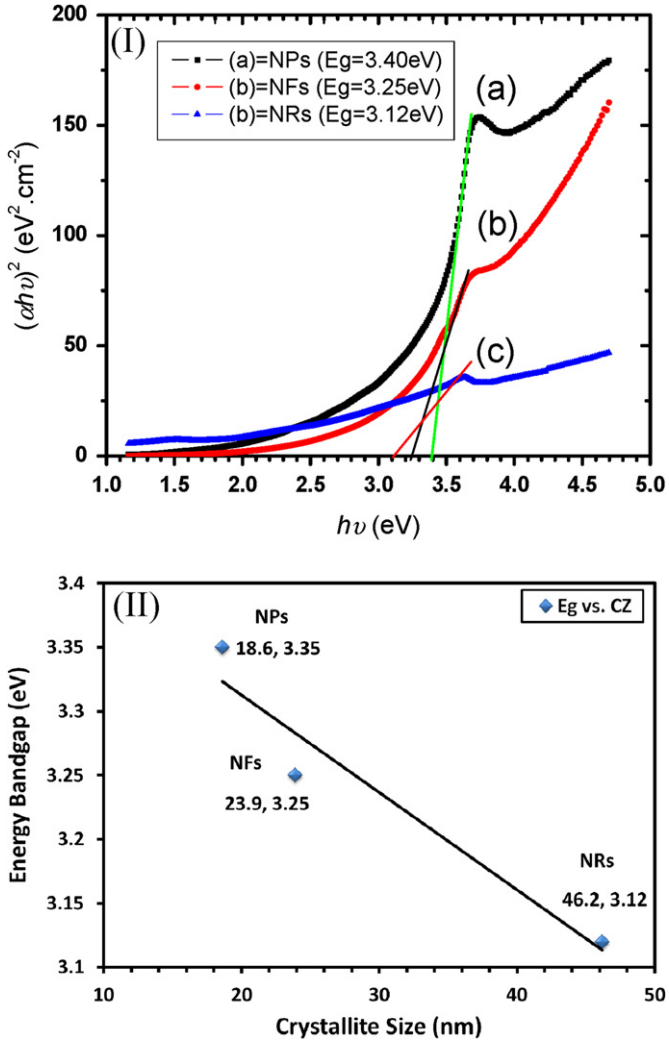

Fig. 10. (I) is the Plots of $(\alpha hv)^2$ against photon energy (hv) given the energy gap (Eg) of ZnO (a) nanoparticles; (b) nanoflowers and (c) nanorods. (II) is the variation of the E_g with the crystallite size (CZ).

electron mass. Sarmah and Kumar [51] have reported an increase of the optical gap from 3.76 to 4.16 eV as the SnO_2 nanoparticles size decreases from 14.5 to 8.5 nm. But the previous results were observed for the nanoparticles of much smaller sizes. Consequently, the blue-shift of the energy gap as the grain size decreases cannot be used to explain the observed variation of the optical gap in our case. We believe that the observed difference of the optical band gap may be related to the variation of the stoichometry of ZnO samples and the concentration of the point defects associated with them [52]. Dutta et al. [53] have reported a significant change in optical band gap of ZnO due to defects which discrete states or increase localized energy levels within the band gap.

4. Conclusions

A comparative study between three different morphologies of ZnO nanostructures, namely nanoparticles (NPs), nanoflowers (NFs) and nanorods (NRs) was studied. The XRD results and calculated texture coefficient (T_c) of three morphologies showed that the preferred crystallite orientation in three morphologies is [0 0 2] direction which is the highest in case ZnO NFs. It is shown using FESEM that nanoparticles of ZnO nanostructures have approximately spherical shapes, irregular in shape and size, and very smooth surfaces. However, ZnO nanoflowers have respectable, six petals grown in the medial part of the respectable. XPS results indicated that Zn 2p lines in ZnO nanorods have highest binding energy. Also, the optical properties of three morphologies of ZnO nanostructures were analyzed and confirmed that crystallites of bigger sizes have smallest value of energy band gap. The obtained results are in accordance with experimental [23], theoretical [24] and others [36,38,44–48] available in the literature.

Acknowledgements

The authors would like to thank Universiti Kebangsaan Malaysia (UKM) for supporting this work through grant no: UKM-AP-NBT-15–2010 and DIP-2012-32. The author (Y.A.) would like to acknowledge FRGS grants numbered: 9003-00249 & 9003-00255 and TWAS-Italy, for their full support of his visit to JUST-Jordan under TWAS-UNESCO.

References

[1] F. Hamdani, A. Botchkarev, W. Kim, H. Morkoc, M. Yeadon, J.M. Gibson, S.C.Y. Tsen, D.J. Smith, D.C. Reynolds, D.C. Look, Optical properties of GaN grown on ZnO by reactive molecular beam epitaxy, Applied Physics Letters 70 (1997) 467–469.
[2] K. Nomura, H. Ohta, K. Ueda, T. Kamiya, M. Hirano, H. Hosono., Thin-film transistor fabricated in single-crystalline transparent oxide semiconductor, Science 300 (2003) 1269–1272.
[3] M.H. Huang, S. Mao, H. Feick, H. Yan, Y. Wu, H. Kind, E. Weber, R. Russo, P. Yang., Room-temperature ultraviolet nanowire nanolasers, Science 292 (2001) 1897–1899.
[4] C.T. Lee, Y.K. Su, H.M. Wang, Effect of *rf* sputtering parameters on ZnO films deposited onto GaAs substrates, Thin Solid Films 150 (1987) 283–289.
[5] H.Y. Dang, J. Wang, S.S. Fan, The synthesis of metal oxide nanowires by directly heating metal samples in appropriate oxygen atmospheres, Nanotechnology 14 (2003) 738.
[6] X. Fu, L.A. Clark, Q. Yang, M.A. Anderson, Enhanced photocatalytic performance of titania-based binary metal oxides: TiO_2/SiO_2 and TiO_2/ZrO_2, Environmental Science and Technology 30 (1996) 647–653.
[7] R.F. Service, Materials science: will UV lasers beat the blues?, Science 276 (1997) 895
[8] H. Zhang, D. Yang, X. Ma, Y. Ji, J. Xu, D. Que, Synthesis of flower-like ZnO nanostructures by an organic-free hydrothermal process, Nanotechnology 15 (2004) 622.
[9] K. Keis, E. Magnusson, H. Lindström, S.E. Lindquist, A. Hagfeldt, A 5% efficient photoelectrochemical solar cell based on nanostructured ZnO electrodes, Solar Energy Materials and Solar Cells 73 (2002) 51–58.
[10] V.C. Sousa, A.M. Segadaes, M.R. Morelli, R. Kiminami, Combustion synthesized ZnO powders for varistor ceramics, International Journal of Inorganic Materials 1 (1999) 235–241.
[11] D.S. King, R.M. Nix, Thermal stability and reducibility of ZnO and Cu/ZnO catalysts, Journal of Catalysis 160 (1996) 76–83.

[12] W.J.E. Beek, M.M. Wienk, R.A.J. Janssen, Efficient hybrid solar cells from zinc oxide nanoparticles and a conjugated polymer, Advanced Materials 16 (2004) 1009–1013.
[13] W.J.E. Beek, M.M. Wienk, R.A.J. Janssen, Hybrid polymer solar cells based on zinc oxide, Journal of Materials Chemistry 15 (2005) 2985–2988.
[14] A. Qurashi, N. Tabet, M. Faiz, T. Yamzaki, Ultra-fast microwave synthesis of ZnO nanowires and their dynamic response toward hydrogen gas nanoscale, Research Letters 4 (2009) 948–954.
[15] X.J. Zheng, X.C. Cao, J. Sun, B. Yuan, Q.H. Li, Z. Zhu, Y. Zhang, A vacuum pressure sensor based on ZnO nanobelt film, Nanotechnology 22 (2011) 435501.
[16] M. Rezapour, N. Talebian, Comparison of structural; optical properties and photocatalytic activity of ZnO with different morphologies: effect of synthesis methods and reaction media, Materials Chemistry and Physics 129 (2011) 249–255.
[17] W.L. Lu, P.K. Hung, C.I. Hung, C.H. Yeh, M.P. Houng, Improved optical transmittance of Al-doped ZnO thin films by use of ZnO nanorods, Materials Chemistry and Physics 130 (2011) 619–623.
[18] C.L. Tsai, Y.C. Tseng, W.M. Cho, Y.J. Lin, H.C. Chang, Y.H. Chen, C.H. Lin, Effects of ultraviolet treatment on the optical and structural properties of ZnO nanoparticles, Materials Chemistry and Physics 130 (2011) 299–302.
[19] B. Cheng, X. Wang, L. Liu, L. Guo, Growth mechanism and morphology dependent luminescence properties of ZnO nanostructures prepared in aqueous solution, Materials Letters *62* (2008) 3099–3102.
[20] P. Li, H. Liu, Y.F. Zhang, Y. Wei, X.K. Wang, Synthesis of flower-like ZnO microstructures via a simple solution route, Materials Chemistry and Physics 106 (2007) 63–69.
[21] J. Liu, X. Huang, Y. Li, J. Duan, H. Ai, Large-scale synthesis of flower-like ZnO structures by a surfactant-free and low-temperature process, Materials Chemistry and Physics 98 (2006) 523–527.
[22] A. Jana, N.R. Bandyopadhyay, P.S. Devi, Formation and assembly of blue emitting water lily type ZnO flowers, Solid State Sciences 13 (2011) 1633–1637.
[23] K. Hummer, Interband magnetoreflection of ZnO, Physica Status Solidi B Basic Solid State Physics 56 (1973) 249–260.
[24] Z. Charifi, H. Baaziz, A.H. Reshak, Ab-initio investigation of structural; electronic and optical properties for three phases of ZnO compound, Physica Status Solidi B Basic Solid State Physics 244 (2007) 3154–3167.
[25] C. Barret, T.B. Massalski, Structure of Metals, Pergamon, Oxford, 1980, p. 204.
[26] R. Romero, D. Leinen, E.A. Dalchiele, J.R. Ramos-Barrado, F. Martín, The effects of zinc acetate and zinc chloride precursors on the preferred crystalline orientation of ZnO and Al-doped ZnO thin films obtained by spray pyrolysis, Thin Solid Films 515 (2006) 1942–1949.
[27] M.M. Bagheri-Mohagheghi, N. Shahtahmasebi, M.R. Alinejad, A. Youssefi, M. Shokooh-Saremi, The effect of the post-annealing temperature on the nano-structure and energy band gap of SnO_2 semiconducting oxide nano-particles synthesized by polymerizing-complexing sol–gel method, Physica B 403 (2008) 2431–2437.
[28] S. Ghosh, A. Mukherjee, H. Kim, C. Lee, Influence of annealing on the structural properties of chemically synthesized CdS nanocrystallites, Materials Chemistry and Physics 78 (2003) 726–732.
[29] R. Al-Gaashani, S. Radiman, N. Tabet, A.R. Daud, Effect of microwave power on the morphology and optical property of zinc oxide nano-structures prepared via a microwave-assisted aqueous solution method, Materials Chemistry and Physics 125 (2011) 846–852.
[30] Y.C. Liang, Growth and physical properties of three-dimensional flower-like zinc oxide microcrystals, Ceramics International 38 (2012) 1697–1702.
[31] M.G. Ma, Y.J. Zhu, G.F. Cheng, Y.H. Huang, Microwave synthesis and characterization of ZnO with various morphologies, Materials Letters 62 (2008) 507–510.
[32] C.D. Wagner, L.H. Gale, R.H. Raymond, Two-dimensional chemical state plots: a standardized data set for use in identifying chemical states by X-ray photoelectron spectroscopy, Analytical Chemistry 51 (1979) 466–482.
[33] H. Zhou, Z. Li, Synthesis of nanowires; nanorods and nanoparticles of ZnO through modulating the ratio of water to methanol by using a mild and simple solution method, Materials Chemistry and Physics 89 (2005) 326–331.
[34] M.J. Gladys, I. Ermanoski, G. Jackson, J.S. Quinton, J.E. Rowe, T.E. Madey, A high resolution photoemission study of surface core-level shifts in clean and oxygen-covered I_r(2 1 0) surfaces, Journal of Electron Spectroscopy and Related Phenomena 135 (2004) 105–112.
[35] J.H. Zheng, Q. Jiang, J.S. Lian, Synthesis and optical properties of flower-like ZnO nanorods by thermal evaporation method, Applied Surface Science 257 (2011) 5083–5087.
[36] J.F. Moulder, W.F. Stickle, P.E. Sobol, K.D. Bomben, in: J. Chastain (Ed.), Handbook of X-ray Photoelectron Spectroscopy, Perkin-Elmer Corporation, Eden Prairie; MN; USA, 1992, p. 89.
[37] J. Das, S.K. Pradhan, D.R. Sahu, D.K. Mishra, S.N. Sarangi, B.B. Nayak, S. Verma, B.K. Roul, Micro-Raman and XPS studies of pure ZnO ceramics, Physica B 405 (2010) 2492–2497.
[38] J. Lee, J. Chung, S. Lim, Improvement of optical properties of post-annealed ZnO nanorods, Physica E 42 (2010) 2143–2146.
[39] A.A. Tahir, V. McKee, Nanostructured α-Fe_2O_3 thin films for photoelectrochemical hydrogen generation, Chemistry of Materials 21 (2009) 3763.
[40] F.K. Shan, B.I. Kim, G.X. Liu, Z.F. Liu, J.Y. Sohn, W.J. Lee, B.C. Shin, Y.S. Yu, Blue shift of near band edge emission in Mg doped ZnO thin films and aging, Journal of Applied Physics 95 (2004) 4772–4776.
[41] J. Tauc, Amorphous and Liquid Semiconductors, Plenum, London; New York, 1974.
[42] K. Morigaki, Physics of Amorphous Semiconductors Imperial, College Press London; World Scientific Pub Co Inc, 1999.
[43] A.D. Yoffe, Low-dimensional systems: quantum size effects and electronic properties of semiconductor microcrystallites zero-dimensional systems and some quasi-two-dimensional systems, Advances in Physics 42 (1993) 173–262.
[44] J. Pal, P. Chauhan, Structural and optical characterization of tin dioxide nanoparticles prepared by a surfactant mediated method, Mater Characterization 60 (2009) 1512–1516.
[45] R. Reisfeld, Nanosized semiconductor particles in glasses prepared by the sol–gel method: their optical properties and potential uses, Journal of Alloys and Compounds 341 (2002) 56–61.
[46] K.F. Lin, H.M. Cheng, H.C. Hsu, L.J. Lin, W.F. Hsieh, Band gap variation of size-controlled ZnO quantum dots synthesized by sol–gel method, Chemical Physics Letters 409 (2005) 208–211.
[47] H. Kou, X. Zhang, Y. Du, W. Ye, S. Lin, C. Wang, Electrochemical synthesis of ZnO nanoflowers and nanosheets on porous Si as photoelectric materials, Applied Surface Science 257 (2011) 4643–4649.
[48] S. Lee, J.W. Peng, C.Y. Ho, Reversible tuning of ZnO optical band gap by plasma treatment, Materials Chemistry and Physics 131 (2011) 211–221.
[49] J. Pal, P. Chauhan, Structural and optical characterization of tin dioxide nanoparticles prepared by a surfactant mediated method, Materials Characterization 60 (2009) 1512–1516.
[50] A. Sharma, D. Prakash, K.D. Verma, Optical characterization of hydrothermally grown SnO_2 nanocrystals, Journal of Optoelectronics and Adavnced Materials 11 (2009) 331–337.
[51] S. Sarmah, A. Kumar, Optical properties of SnO_2 nanoparticles, Indian Journal of Physics 84 (2010) 1211–1221.
[52] R. Al-Gaashani, S. Radiman, N. Tabet, A.R. Daud, Optical properties of SnO_2 nanostructures prepared via one-step thermal decomposition of tin (II) chloride dihydrate, Materials Science and Engineering B 177 (2012) 462–470.
[53] S. Dutta, S. Chattopadhyay, A. Sarkar, M. Chakrabarti, D. Sanyal, D. Jana, Role of defects in tailoring structural; electrical and optical properties of ZnO, Progress in Materials Science 54 (2009) 89–136.